

Magnesium-Vacancy Optical Centers in Diamond

Original

Magnesium-Vacancy Optical Centers in Diamond / Corte, Emilio; Andrini, Greta; Nieto Hernández, Elena; Pugliese, Vanna; Costa, Ângelo; Magchiels, Goele; Moens, Janni; Tunhuma, Shandirai Malven; Villarreal, Renan; Pereira, Lino M. C.; Vantomme, André; Correia, João Guilherme; Bernardi, Ettore; Traina, Paolo; Degiovanni, Ivo Pietro; Moreva, Ekaterina; Genovese, Marco; Ditalia Tchernij, Sviatoslav; Olivero, Paolo; Wahl, Ulrich; Forneris, Jacopo. - In: ACS PHOTONICS. - ISSN 2330-4022. - 10:1(2022), pp. 101-110. [10.1021/acsphotonics.2c01130]

Availability:

This version is available at: 11583/2974307 since: 2023-02-03T09:51:07Z

Publisher:

American Chemical Society

Published

DOI:10.1021/acsphotonics.2c01130

Terms of use:

This article is made available under terms and conditions as specified in the corresponding bibliographic description in the repository

Publisher copyright

ACS postprint/Author's Accepted Manuscript

This document is the Accepted Manuscript version of a Published Work that appeared in final form in ACS PHOTONICS, copyright © American Chemical Society after peer review and technical editing by the publisher. To access the final edited and published work see <http://dx.doi.org/10.1021/acsphotonics.2c01130>.

(Article begins on next page)

Magnesium-vacancy optical centers in diamond

Emilio Corte^{1,2,3§}, Greta Andrini^{4,2,3§}, Elena Nieto Hernández^{1,2,3}, Vanna Pugliese¹, Ângelo Costa⁵, Goele Magchiels⁵, Janni Moens⁵, Shandirai Malven Tunhuma⁵, Renan Villarreal⁵, Lino M.C. Pereira⁵, André Vantomme⁵, João Guilherme Correia⁶, Ettore Bernardi³, Paolo Traina³, Ivo Pietro Degiovanni^{3,2}, Ekaterina Moreva³, Marco Genovese^{3,2}, Sviatoslav Ditalia Tchernij^{2,1,3}, Paolo Olivero^{1,2,3}, Ulrich Wahl^{6*}, Jacopo Forneris^{1,2,3,*}

¹ Physics Department, University of Torino, Torino 10125, Italy

² Istituto Nazionale di Fisica Nucleare (INFN), Sezione di Torino, Torino 10125, Italy

³ Istituto Nazionale di Ricerca Metrologica (INRiM), Torino 10135, Italy

⁴ Dipartimento di Elettronica e Telecomunicazioni, Politecnico di Torino, Torino 10129, Italy

⁵ KU Leuven, Quantum Solid State Physics, 3001 Leuven, Belgium

⁶Centro de Ciências e Tecnologias Nucleares, Departamento de Engenharia e Ciências e Engenharias Nucleares, Instituto Superior Técnico, Universidade de Lisboa, 2695-066 Bobadela LRS, Portugal

Abstract

We provide the first systematic characterization of the structural and photoluminescence properties of optically active centers fabricated upon implantation of 30-100 keV Mg^+ ions in synthetic diamond. The structural configurations of Mg-related defects were studied by the electron emission channeling technique for short-lived, radioactive ^{27}Mg implantations at the CERN-ISOLDE facility, performed both at room-temperature and 800 °C, which allowed the identification of a major fraction of Mg atoms (~30-42%) in sites which are compatible with the split-vacancy structure of the MgV complex. A smaller fraction of Mg atoms (~13-17%) was found on substitutional sites. The photoluminescence emission was investigated both at the ensemble and individual defect level in the 5-300 K temperature range, offering a detailed picture of the MgV-related emission properties and revealing the occurrence of previously unreported spectral features. The optical excitability of the MgV center was also studied as a function of the optical excitation wavelength to identify the optimal conditions for photostable and intense emission. The results are discussed in the context of the preliminary experimental data and the theoretical models available in the literature, with appealing perspectives for the utilization of the tunable properties of the MgV center for quantum information processing applications.

Keywords

diamond, ion implantation, magnesium, color centers, emission channeling, lattice location

* Corresponding authors: jacopo.forneris@unito.it, uwahl@ctn.tecnico.ulisboa.pt

§ These authors contributed equally to the work.

1. Introduction

Diamond is a promising material platform for photonic quantum technologies, which offers single-photon sources for quantum information processing and sensing schemes based on the optical activity of lattice defects. These systems, commonly known as “color centers”, can be engineered upon the controlled introduction of impurities in the diamond crystal structure by ion implantation¹⁻³. Besides the well-known and widely investigated negatively-charged nitrogen-vacancy center (NV⁻), offering unique photophysical properties (photo-stability at room temperature, high quantum efficiency, optically addressable spin properties) for quantum sensing and computing applications⁴⁻⁹, additional single-photon emitting color centers with appealing features have emerged in the last decade, including group-IV impurities¹⁰⁻¹⁸, noble gases¹⁹⁻²¹ and other impurity-related defects²²⁻²⁴.

Particularly, a recent work has shown a preliminary demonstration of the optical activity of Mg-related color centers in diamond. The available experimental data suggested the formation of an optically active defect (magnesium-vacancy center, MgV in the following) upon Mg ion implantation and annealing, denoted by a sharp emission line at 557.4 nm, low phonon coupling denoted by a high Debye-Waller factor, high (>0.5 Mcps) emission intensity²⁵ and 2-3 ns radiative lifetime. Furthermore, these results fed the deployment of a detailed numerical ab-initio study of the color center’s structure²⁶, offering an intriguing insight in its opto-physical properties, including the prediction of a large and tunable and spin-dependent ground state splitting, thus offering an appealing tool for quantum information processing purposes.

In this work, we report on a systematic investigation of the MgV color center in diamond. The analysis covers both its structural properties and efficiency of structural formation, as evidenced from the determination of the lattice sites of implanted Mg by emission channeling technique, and the optical emission properties, studied in photoluminescence (PL) regime at the ensemble and single-photon emitter level, as a function of temperature and excitation wavelength. The present results extend the preliminary findings available in the scientific literature and offer a contextual evidence to support the theoretical model predicted in Ref. 26.

2. Results

2.a Structural properties of Mg-related defects in diamond

For lattice location determination of Mg in diamond, the electron emission channeling (EC) technique from radioactive isotopes was adopted²⁷⁻³⁰ (**Fig. S1** of Supporting Information). The EC method allows probing the sites of radioactive isotopes in single-crystalline samples, and was recently applied to identify the split-vacancy configuration of implanted ¹²¹Sn inside the SnV complex in diamond³¹. The split vacancy configuration can be pictured as the impurity atom in the center of a divacancy, occupying a position which corresponds to the bond center (BC) site in an unperturbed lattice. The radioactive probe atoms are implanted at low fluences and the emitted β^- particles are guided by the crystal

potential on their way out of the crystal. A two-dimensional position-sensitive detector (PSD)^{28,29} is used to measure the angle-dependent emission yield of electrons in the vicinity of major crystallographic directions, providing patterns which are characteristic for the probe atom lattice location in the sample. In the case of Mg, we used the short-lived ²⁷Mg ($t_{1/2}=9.45$ min), which was produced at CERN's ISOLDE on-line isotope separator facility by means of bombarding Ti targets with 1.4 GeV protons, followed by out-diffusion, resonant laser ionization and mass separation. More experimental details regarding EC experiments with ²⁷Mg can be found in Refs. 32, 33 and in the Supporting Information. The major lattice sites can be identified by fitting the experimentally observed emission yields by linear combinations of theoretical patterns^{28,29,34} calculated for specific positions of the emitter atoms in the lattice. For that purpose, the many-beam approach^{27,28} was used to calculate the expected emission yields for substitutional (*S*) as well as around 250 interstitial sites in the diamond structure, which are obtained by displacing from the *S* position along $\langle 111 \rangle$, $\langle 100 \rangle$, or $\langle 110 \rangle$ directions in steps of around 0.04 Å (**Fig. S3** of Supporting Information).

The sample used for the EC studies was a $\langle 100 \rangle$ oriented single crystal from ElementSix, termed “SC plate CVD”, of size 3.0×3.0×0.25 mm³, with nitrogen concentration [N] < 1 ppm. Implantations were performed with 30 keV into a 1-mm diameter beam spot, simultaneously with the measurement of β^- emission channeling effects by a 30×30 mm² PSD placed at a distance of 301 mm from the sample, resulting in an angular resolution of $\sim 0.1^\circ$ (standard deviation). The fluences used to measure single EC patterns were around 2.1-5.5×10¹¹ cm⁻², while the total accumulated fluence at the end of the experiment was 1.1×10¹³ cm⁻².

The half-life of ²⁷Mg is too short to perform annealing at high temperatures; with regard to thermal treatment of the sample the only feasible option is varying the implantation temperature. The experimental emission patterns around $\langle 110 \rangle$, $\langle 211 \rangle$, $\langle 100 \rangle$ and $\langle 111 \rangle$ directions during room temperature (RT) implantation are shown in **Fig. 1a-d**, those for 800 °C implantation (<10⁻⁵ hectopascal pressure) in **Fig. 2a-d**. As a first qualitative observation we notice that anisotropies of the EC effects measured from ²⁷Mg are relatively weak in comparison to effects from other elements implanted under similar conditions into diamond, e.g. those of ¹²¹Sn.³¹ This indicates that a considerable fraction of emitter atoms occupies lattice sites of relatively low crystal symmetry. In a first approach for the analysis, the experimental patterns were fitted by allowing two fractions (“2-site fits”) of emitter atoms, one on ideal substitutional *S* and another on ideal bond-center (BC) sites, plus a flat contribution, which always needs to be considered in the analysis of EC patterns (the theoretical emission patterns for *S* and BC sites are shown in **Fig. S4** of Supporting Information). The resulting best fit patterns for $\langle 110 \rangle$, $\langle 211 \rangle$, $\langle 100 \rangle$ are shown in **Fig. 1e-g** and **Fig. 2e-g**. As was outlined previously,³¹ in the case of the $\langle 111 \rangle$ direction, the patterns from *S* and BC sites have qualitatively similar features, which results in the corresponding site fractions of the best fits being unstable. The theoretical patterns included for the $\langle 111 \rangle$ direction in **Figs 1h** and **2h** are hence not those for the best fit results of that direction, but for relative contributions from *S* and BC sites that were fixed to the ratios derived from the analysis of the other three directions (cf. Supporting Information). In all cases the simulated patterns satisfactorily match the experimental results; the $\langle 111 \rangle$ measurements are also compatible with the results from the other directions. Compared to 1-site fits using either *S* or BC positions, the 2-site fits with *S* and BC significantly

improved the chi square of the fit by 19-42%, and by 17–53%, respectively, while for the $\langle 111 \rangle$ directions the improvement was much smaller, 1-3% only.

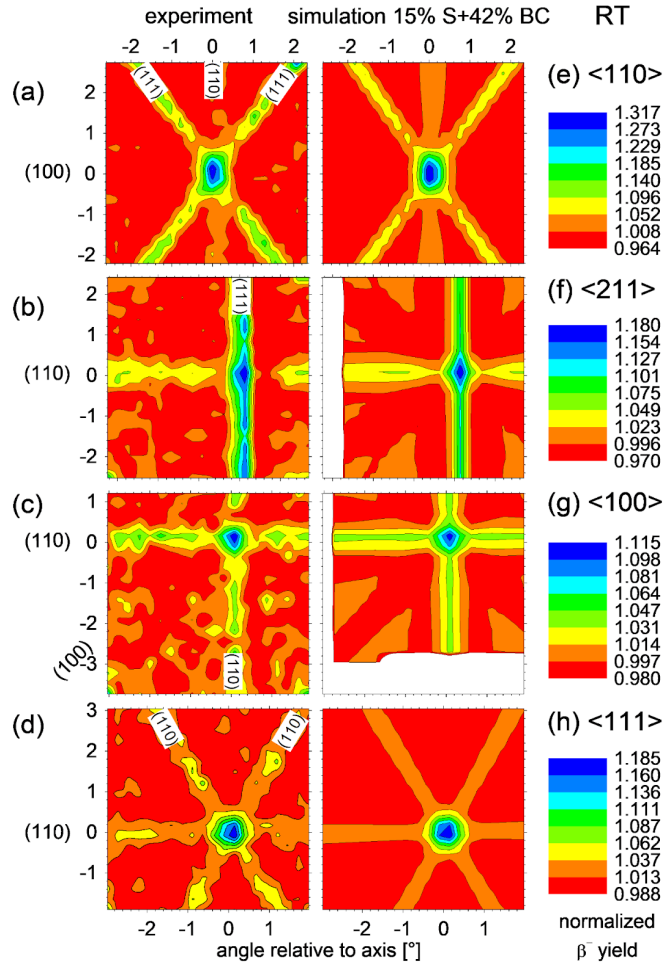


Figure 1: a)-d) Experimental β^- emission channeling patterns from ^{27}Mg in diamond around the $\langle 110 \rangle$, $\langle 211 \rangle$, $\langle 100 \rangle$, and $\langle 111 \rangle$ directions during RT implantation. The panels show the number of detected electrons (normalized intensity indicated by the color scales) as a function of the angle relative to the respective crystal axis. These patterns are a signature for the exact location of the probe atom in the diamond lattice. The plots e)-h) are simulated theoretical patterns considering 15% on ideal substitutional and 42% on ideal bond-center sites. Note that during the RT $\langle 211 \rangle$ and $\langle 100 \rangle$ measurements the sample was not yet oriented in such a way that the calculated patterns $[\pm 3.0^\circ]$ cover the whole range of measured angles. The areas in the simulated patterns f) and g) which are not covered, are shown in white.

For both implantation temperatures, the largest fitted fractions were on bond-center sites (42% at RT, 30% at 800 °C), while smaller fractions were assigned to the substitutional positions (15% at RT, 14% at 800 °C). The result implies that 30-40% of implanted Mg atoms are found on sites which are compatible with the theoretically predicted Mg position within the MgV defect in the split-vacancy configuration of D_{3d} symmetry.²⁶ From a comparison of fluorescence intensity and implanted fluence, the formation efficiency of *optically active* MgV centers had been estimated as 2-3% in undoped diamond implanted at RT and annealed to 800 °C.³⁵ Our results show that the *structural* efficiency of formation of the split-vacancy configuration in undoped diamond is certainly much higher than a few

percent only, suggesting that a large part of the MgV centers are *optically inactive*. The fact that significantly higher optical activation was observed in P-doped diamond, reaching values as high as 48% following 1200 °C annealing,³⁵ indicates that co-doping with the n-type dopant P may transform an inactive form of MgV into optically active MgV centers. Within the scope of the 2-site fit analysis of the EC experimental data, relatively large fractions of emitter atoms (43% at RT, 56% at 800 °C) were assigned to flat contributions to the emission patterns, the so-called “random sites”. The assignment of random sites cannot be the consequence of significant radiation damage or amorphization of the sample, since for the light mass of ²⁷Mg at the applied fluences, the effect of damage should be negligible in diamond, especially for the implantation temperature of 800 °C. The most likely interpretation is that the random fraction represents additional ²⁷Mg sites

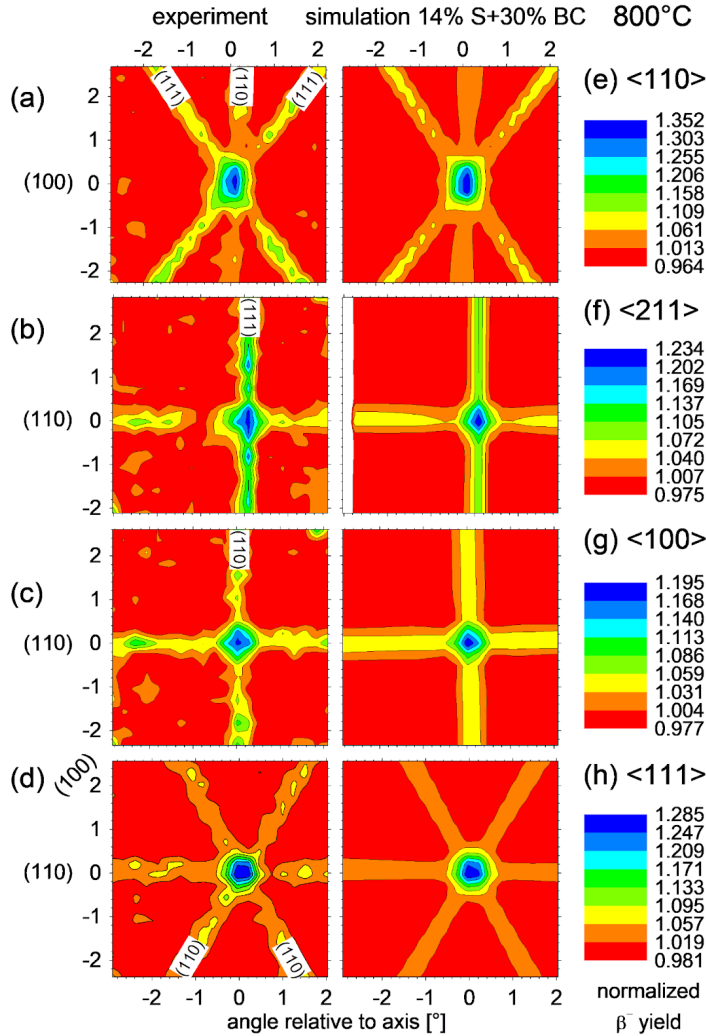


Figure 2: **a)-d)** Experimental β^- emission channeling patterns from ²⁷Mg in diamond around the $\langle 110 \rangle$, $\langle 211 \rangle$, $\langle 100 \rangle$, and $\langle 111 \rangle$ directions during 800 °C implantation. The plots **e)-h)** are simulated theoretical patterns considering 14% on ideal substitutional and 30% on ideal bond-center sites.

of relatively low crystal symmetry, which only produce weak anisotropies in the angular-dependent electron emission yields. Two defect configurations, which could be responsible for such Mg lattice sites, are Mg inside a triple vacancy or inside a quadruple vacancy,

which corresponds to the so-called MgV_2 or MgV_3 complexes (possible structures for these complexes are shown in **Fig. S3** of Supporting Information). MgV_2 was theoretically considered,²⁶ and it was found to have a somewhat higher energy of formation than MgV , which was predicted to be the thermodynamically most stable Mg defect, followed by substitutional Mg. We note, however, that in the case of ion implantation the energy for vacancy creation in the sample is provided by the implantation process, hence the fact that MgV exhibits the lowest defect formation energy may not be the single determining factor which regulates the abundance of complexes formed, and thus also Mg centers requiring triple or quadruple vacancies might be commonly found. The MgV_2 center was predicted to have a similar configuration as the MgV , with an additional vacancy “attached from the side” and a symmetry lowering to C_1 (although no detailed Mg coordinates were published).²⁶ From simple geometrical arguments, one might expect the structure of MgV_2 as a central vacancy with two additional nearest-neighbor single vacancies within a (110) plane, and hence with the Mg atom displaced along a $\langle 100 \rangle$ direction from an S site (**Fig. S3**). In the case of MgV_3 , there exist no predictions for its structure or formation energy in the literature. From simple geometric arguments, for Mg inside a quadruple vacancy consisting of one missing C atom with three additional nearest-neighbor single vacancies, one would tentatively expect trigonal symmetry with the Mg atom located close to the so-called anti-bonding (AB) position (**Fig. S3**).

Having these intuitive structures of MgV_2 and MgV_3 in mind, and considering the possible existence of isolated interstitial Mg, we performed 3-site fits where, besides Mg on S and BC sites, the position of a third fraction of Mg probes was varied. We did not find any indication for the existence of (isolated) tetrahedral interstitial Mg (T_d symmetry), which supports the theoretical prediction that this configuration has a high formation energy, making it particularly unstable in vacancy-rich ion-implanted diamond. However, while the chi square of the $\langle 110 \rangle$ and $\langle 211 \rangle$ pattern fits improved if Mg sites displaced along $\langle 100 \rangle$ from S sites were considered, this result could not be confirmed by the $\langle 100 \rangle$ patterns. The identification of a third fraction of Mg probes in highly symmetric lattice sites, in particular displaced from S along $\langle 100 \rangle$ directions, was hence not conclusive. An attempt will be made to resolve further Mg lattice sites by means of EC experiments using enhanced angular resolution of 0.05° .

2b. Optical properties of MgV centers

Spectral features of ensemble photoluminescence. The detailed optical characterization of MgV centers was performed on a set of $2 \times 2 \times 0.5 \text{ mm}^3$ IIA single-crystal diamond plates produced by ElementSix by Chemical Vapor Deposition method. The crystals were denoted as “electronic grade” by the supplier, according to the nominal substitutional N and B concentrations below 5 ppb. The sample was implanted with 100 keV $^{24}\text{Mg}^+$ ions at the IMBL laboratory (KU Leuven). Several squared regions of $\sim 200 \mu\text{m}$ edge were irradiated at different fluences in the $5 \times 10^9 - 5 \times 10^{12} \text{ cm}^{-2}$ range through the utilization of a custom Al implantation mask ($\sim 15 \mu\text{m}$ thickness). The sample was then processed with a high-temperature thermal annealing (1200 °C, 2 hours at $\sim 10^{-6}$ hectopascal pressure) and a subsequent oxygen plasma treatment, with the purpose of minimizing the background fluorescence originating from surface contaminants. The room-temperature PL emission spectrum of the highest-fluence Mg-implanted diamond ($5 \times 10^{12} \text{ cm}^{-2}$) was acquired using

a confocal micro-Raman setup under 532 nm excitation wavelength (21.6 mW optical power, <0.1 nm resolution, **Fig. 3a**). The ensemble emission highlighted the following spectral features:

- a sharp line at 572.8 nm corresponding to the first-order Raman scattering of diamond (1332 cm^{-1} shift);

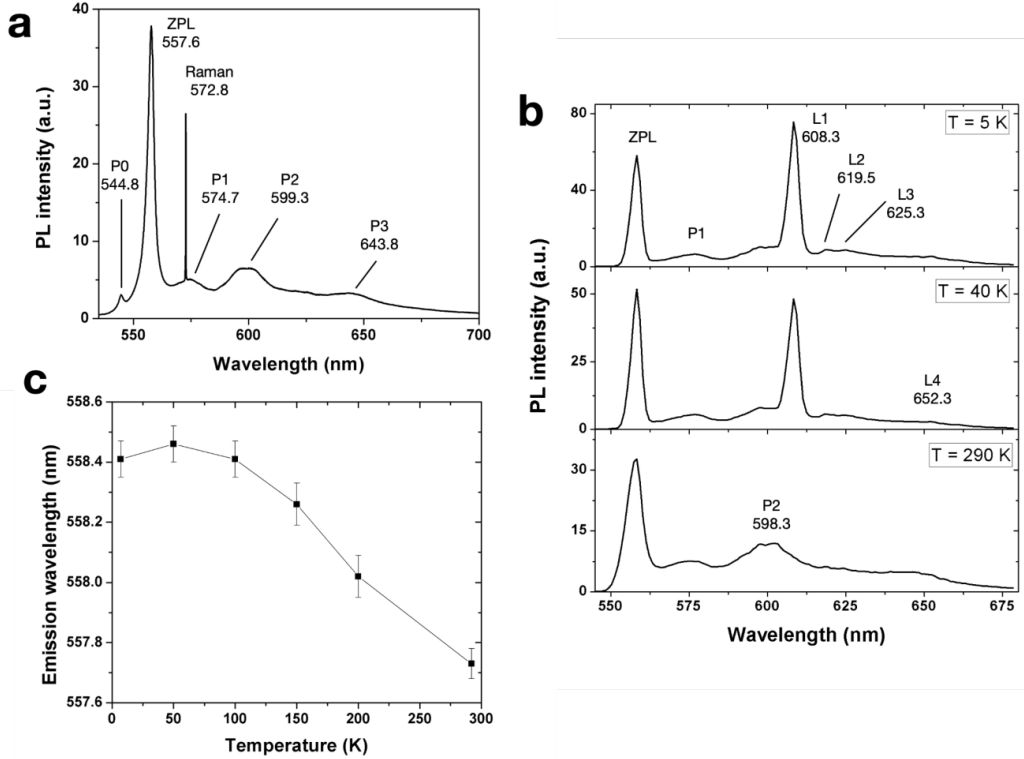


Figure 3: a) RT spectrum of MgV ensemble ($5 \times 10^{12}\text{ cm}^{-2}$ implantation fluence) upon 532 nm laser excitation. b) Ensemble spectra acquired under 522 nm excitation (3.7 mW) at 5 K, 40 K, 290 K temperature. c) Nominal position of the MgV ZPL dependence on the temperature.

- an intense emission peak at 557.6 nm (2.224 eV; 3 nm FWHM), whose prominence with respect to all the remaining spectral features is in agreement with the early reports on its attribution to the zero-phonon line (ZPL) of the MgV defect^{25,35} and its theoretical prediction as the main emission of the color center in its negative charge state.²⁶

- a set of significantly less intense PL peaks centered at 574.7 nm (2.158 eV, denoted as “P1” in the following), 599.3 nm (2.069 eV P2) and 643.8 nm (1.926 eV, P3). The wavelength of these three bands is compatible with the phonon sideband spectrum of the MgV center predicted in Ref 26.

- an additional emission line at 544.8 nm (2.28 eV, “P0” in the following), exhibiting higher emission energy with respect to the MgV ZPL. The origin of such a feature is not clear. Its correlation with Mg-related emission in n-type diamond³⁵ is questioned by its observation in this work in undoped, highly pure substrates. Furthermore, no explicit observation in irradiated or ion-implanted diamond is present in the scientific literature to support its attribution to an intrinsic radiation-induced defect. The peak could thus be interpreted either as a Mg-vacancy complex different from the MgV center, in analogy with the 593.5

nm line in Sn-implanted diamond,¹⁵ or, less likely, to the predicted ground-state splitting of the MgV defect.²⁶ In the latter case, however, the observed splitting (~52 meV) would greatly exceed the expected value of 22 meV.

A further temperature dependent study on PL spectra (5-300 K range, 522 nm excitation, **Fig. 3b**) from the same MgV ensemble offered two additional insights in the optical activity of such a lattice complex.

Firstly, the MgV ZPL spectral shift exhibited a wavelength increase at decreasing temperatures. This effect is shown in **Fig. 3c**, which reports the central wavelength of the ZPL (whose uncertainty of ~0.2 nm was estimated with the uncertainty associated with the Gaussian centroid fitting parameter) as a function of temperature. The shift was quantifiable in ~1 nm (558.4 nm) at 5 K with respect to the 557.6 nm emission at room temperature. This observation, to the best of the authors’ knowledge, is unprecedented for a solid-state color center, where the lattice parameter contraction at decreasing temperatures typically corresponds to a strengthening of the chemical bonds, and thus an increase in the photon energy.³⁶⁻³⁹

This observation can be understood on the basis of the *ab-initio* model in Ref. 26, which predicts that the MgV ZPL is an emission doublet originating from a ground state splitting, and that it exhibits decreasing energy separation at increasing compressive strain, hence at decreasing temperature. This prediction is not in contrast with the rather large ~3 nm ZPL peak FWHM measured in the high-resolution PL spectra reported in **Fig. 3a**, which could be interpreted as the convolution of the predicted emission doublet. The blue-shift then would be justified by an increased occupation probability of the ⁴E_u state. High resolution spectroscopy at cryogenic temperatures will be needed to further assess this hypothesis. Secondly, the low temperature emission becomes dominated by a new set of spectral features, namely an intense peak at 608.3 nm (2.038 eV, “L1” in the following), exhibiting an intensity comparable with that of the MgV ZPL, accompanied by a set of weak bands at 619.5 nm (2.001 eV, L2), 625.3 nm (1.983 eV, L3) and 652.3 nm (1.901 eV) which can be tentatively interpreted as L1 phonon replicas.

The L1 line energy is compatible with its attribution to the ²A_{1u} → ²E_g transition, predicted at ~2 eV in Ref. 26. The lack of observation of this line at room temperature is compatible with the fact that it is a weakly-allowed transition. The ~185 meV energy difference between the ²A_{1u} and the ²E_u(²) states (i.e., the excited states of the ZPL and L1 transitions, for which the same final state ²E_g is assumed²⁶) might be sufficient to favor the population of the latter upon room temperature phonon-assisted processes, thus quenching the L1 emission line.

Optical excitability. The ensemble spectral emission of the same Mg-implanted region was investigated under different laser excitation wavelengths (**Fig. 4a-d**), namely 405 nm, 450 nm, 490.5 nm, 509.5 nm (2.2mW) and 522 nm using a fiber-coupled single-photon-sensitive confocal microscope (details on optical filtering and position of the Raman scattering lines are given in the **Supporting Information**).

All the above-mentioned excitation wavelengths highlighted the occurrence of the ZPL and P2-P3 emission lines, thus confirming their attribution to PL features in Mg-implanted diamond rather than Raman-related features of the implanted host material. Differently with respect to the other laser sources, for which a 505 nm long pass filter was used, the excitation spectrum under 522 nm excitation (**Fig. 1b**) was acquired using a 567 nm long-

pass dichroic mirror. In this case, the $\sim 50\%$ transmittance of the filter at 560 nm^{40} was sufficient to observe the ZPL of the MgV center but partially suppressed its emission intensity. Moreover, in the case of 522 nm excitation, the first-order Raman scattering occurs at 561 nm wavelength and thus partially overlaps with the ZPL of the MgV center under the given resolution ($\sim 4\text{ nm}$) of the spectrometry setup. Based on these considerations, a direct comparison in the ZPL intensity acquired under 522 nm laser and that observed at other excitation wavelengths was not possible. It is however worth mentioning that the overall prominence of the MgV ZPL with respect to the baseline under laser excitation in the $405\text{-}510\text{ nm}$ range (for which the same optical setup was employed) decreases at increasing excitation energy, suggesting a progressive conversion between the charge state configurations available within the energy gap of diamond.²⁶ This hypothesis is further supported by the inability to detect single-photon emission under $<510\text{ nm}$ excitation in regions where an abundance of individual centers were identified at longer wavelengths.

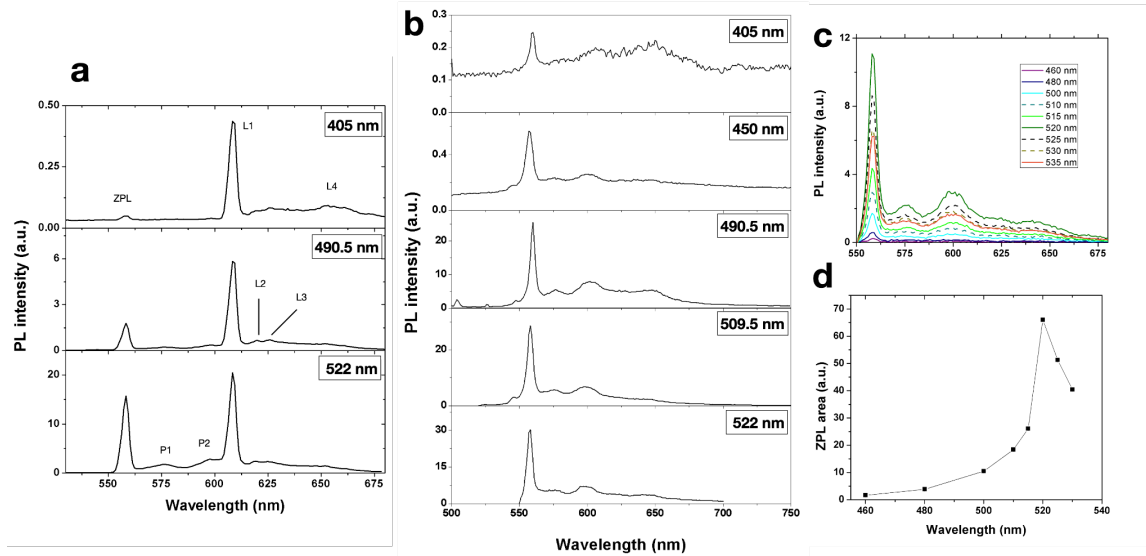


Figure 4: Ensemble spectra acquired: **a)** at 5 K temperature under: 405 nm (3.6 mW optical power), 490.5 nm (4.0 mW), 522 nm (3.6 mW) excitation wavelengths. **b)** at room temperature under **b)** 405 nm (8mW), 450 nm (2.2 mW), 490.5 nm (2.3 mW), 509.5 nm (2.2 mW) and 522 nm excitation wavelengths (0.3 mW). The spectra are normalized to the optical excitation power. **c)** background subtracted spectra acquired under $50\text{ }\mu\text{W}$ pulsed laser excitation (80 MHz repetition rate). **d)** Excitation wavelength dependence of the 556.7 nm ZPL peak area extracted from the spectra in **Figure 2c**.

A further investigation of the dependence of the Mg-related PL on the excitation energy was performed using a dedicated supercontinuum laser source filtered to offer an emission bandwidth of 10 nm with central wavelength in the range $460\text{-}535\text{ nm}$ (see Supplementary information for further details). The different ensemble spectra in **Fig. 4c** were acquired with $50\text{ }\mu\text{W}$ fixed optical power (the data are background-subtracted; the background was measured by acquiring spectra in a pristine region of the sample to remove the contribution originating from Raman scattering). The area subtended by the ZPL peaks, reported in **Fig. 4d**, confirms that the maximum excitability of the MgV emission is at 522 nm , as suggested also by **Fig. 4a-b**. This feature indicates that the chosen wavelength is an effective tool to provide Raman-resonant excitation of the MgV center, thus enabling, in perspective, an

efficient resource to maximize its emission intensity and optically address and coherently control individual emitters⁴¹ using readily available and cost-effective laser diodes.

Single-photon emission analysis. PL measurements on individual MgV centers were performed under 522 nm excitation at the outer edge of a region implanted at a $5 \times 10^{12} \text{ cm}^{-2}$ fluence. **Figure 5a** shows a $7 \times 8 \text{ }\mu\text{m}^2$ map of such a region, acquired in confocal microscopy (1 mW excitation power), where the formation of individual luminescent spots of $\sim 1 \text{ }\mu\text{m}^2$ density is clearly recognizable. A systematic analysis on such individual luminescent spots via Hanbury-Brown & Twiss (HBT) interferometry enabled to identify and analyze single-emitting defects, whose room-temperature characterization was performed in terms of their spectral properties, radiative lifetime of the excited state and intensity saturation emission.

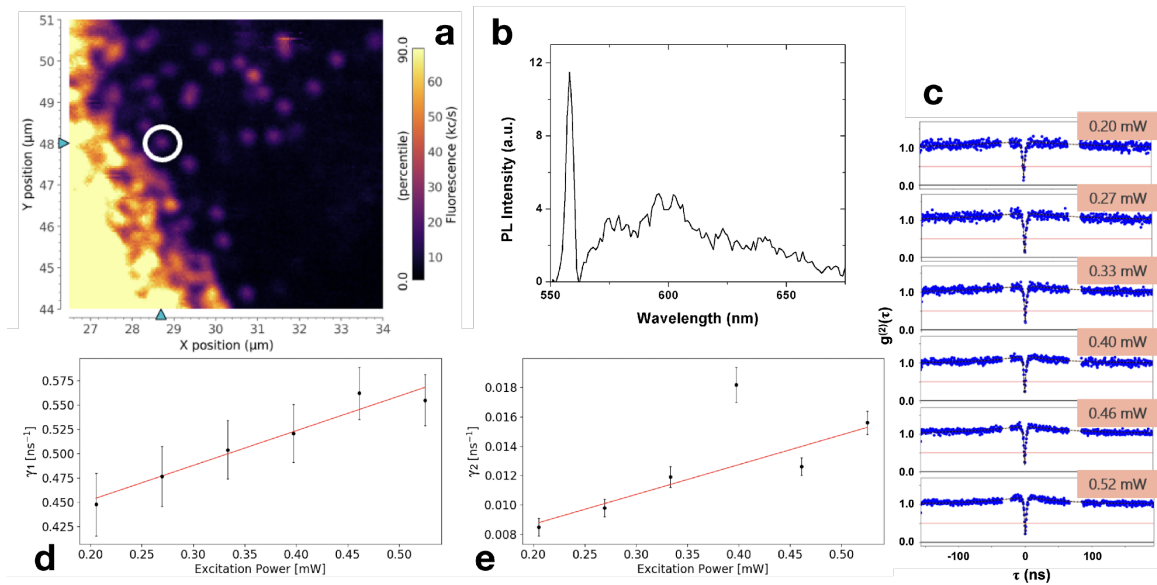


Figure 5: Room-temperature single-photon emission from MgV centers: **a)** Confocal microscopy map acquired under 522 nm laser excitation (1.0 mW) at the outer edge of a region implanted with Mg^+ ions at $5 \times 10^9 \text{ cm}^{-2}$ fluence. **b)** Background-subtracted PL spectrum acquired from the individual emitter circled in white in Fig. 3a. **c)** Second-order auto-correlation function measurements of the same emitter under different optical excitation powers (0.2-0.52 mW range). The missing data points correspond to the backflash peaks originating from the fiber-coupled HBT interferometer, which were removed for clarity. **d)** Dependence of the γ_1 emission parameters on the optical excitation power. **e)** Dependence of the γ_2 emission fitting parameter on the optical excitation power.

As an example, the individual emitter highlighted in **Fig. 5a** by a white circle exhibits the emission spectrum shown in **Fig. 5b**, which was acquired upon subtraction of the background emission acquired in the same experimental conditions from an unimplanted region of the sample. The measurement of the second-order autocorrelation function $g^{(2)}(\tau)$, presented in **Fig. 5c**, was performed under different optical power excitations (0.20-0.52 mW range) highlighting a strong antibunching at a null delay time. This behavior, which indicates the occurrence of non-classical emission, resulted in a background-subtracted value of $g^{(2)}(\tau=0)$ well below 0.5 (0.15 ± 0.10 at 0.27 mW excitation power), which is regarded as the threshold for single-photon emitter discrimination. A bunching effect also became visible at increasing excitation powers, suggesting the presence of a shelving state

involved in the emission dynamics of the center. The background-subtracted $g^{(2)}(\tau)$ curves were fitted (black dashed lines in **Fig. 5b**) according to the $g^{(2)}(\tau)$ model corresponding to a three-level system

$$g^{(2)}(\tau) = 1 - (1 + a) \cdot \exp(-|\tau| \cdot \gamma_1) + a \cdot \exp(-|\tau| \cdot \gamma_2) \quad (1)$$

where γ_1 and γ_2 are reciprocal of the characteristic times associated with the de-excitation of the excited state and the shelving state, respectively.⁴² The radiative lifetime of the center was finally estimated, by a linear fit of the γ_1 parameter against the excitation power P , as $\tau = [\gamma_1(P=0)]^{-1} = (2.7 \pm 0.3)$ ns (**Fig. 5d**).⁴³ A statistical analysis based on 15 individual emitters acquired from the same region (**Fig. 6a**) revealed a relatively small dispersion of the data with a weighted average lifetime of (2.4 ± 0.2) ns, in good agreement with the preliminary data reported in Ref. 25. The fitting function in eq. (1) enabled also to investigate the dependence of the γ_2 parameter on the power of the optical excitation. **Figure 5e** shows the data acquired for the same emitter considered in **Fig. 5c-d**. Notably, a clear increasing trend was observed, and the behavior was consistent for all the 15 emitters analyzed in this work, confirming that the emitter is adequately described by a three-level model.^{43,44} The emission intensity of individual MgV centers was also studied as a function of the optical power of the laser excitation. **Figure 6b** displays the large variability (up to 50% of the distribution average) of the background-subtracted emission rate in saturation regime for an exemplary subset of the emitters analyzed in **Fig. 6a**. The data points were fitted according to the saturation model^{11,45,46}

$$I(P) = I_{\text{sat}} \cdot P / (P + P_{\text{sat}}) \quad (2)$$

in which I is the emission rate and P is laser excitation power. The saturation intensity I_{sat} cannot be regarded as a reliable estimate of the brightness of the MgV center, since a significant part of its ZPL emission is filtered by the 567 nm long-pass dichroic mirror adopted for the confocal microscope implementation. Even without considering the 50% transmittance of the latter at 560 nm, the PL count rate at saturation ranges between (0.44 ± 0.03) Mcps and (1.46 ± 0.17) Mcps (blue and red data in **Fig. 6b**, respectively). If the dichroic mirror losses are taken into account, these results suggest room-temperature emission rates above 2 Mcps, previously unreported for a solid-state quantum emitter without coupling to emission-enhancing cavities. Conversely, the saturation power under 522 nm excitation was estimated in the range (0.87 ± 0.09) – (2.7 ± 0.4) mW. In general, a qualitative trend correlating increasing emission intensity and saturation power could be observed.

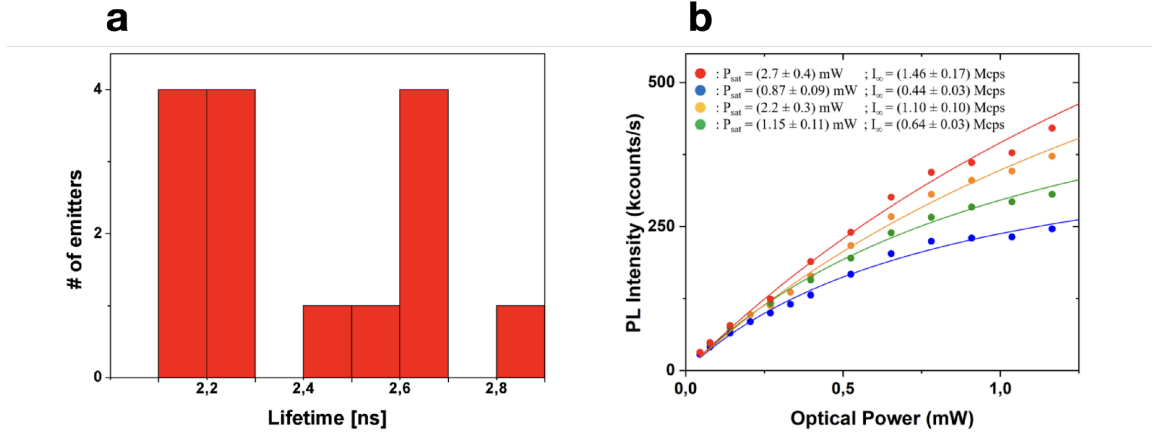


Figure 6: **a)** Distribution of the excited state lifetime of 15 individual MgV centers at room temperature. **b)** Background-subtracted emission rate as a function of the optical excitation power (522 nm wavelength). The colored curves correspond to an exemplary subset of the emitters studied in Fig. 4a. The legend indicates the fitting parameters obtained according to Eq. (2).

The single-photon emission was also investigated at cryogenic temperatures. **Figure 7** shows the typical results obtained for individual color centers at 7 K under 522 nm, excitation. The identification of single MgV emitters was validated by the measurement of the PL spectra (**Fig. 7a**), the evaluation of the $g^{(2)}(0)$ parameter (**Fig. 7b**) (nominally, 0.05 ± 0.01 upon background removal¹⁷) and the excited state lifetime evaluation (**Fig. 7c**) (2.8 ± 1.1 ns). We underline that these results are compatible with what observed in the measurement we carried on at room temperature. Interestingly, the intense L1 emission feature observed from ensemble measurements at cryogenic temperatures could not be identified at the single-photon emitter level. Conversely, dedicated studies at varying excitation wavelengths did not succeed at isolating individual color centers, thus confirming the analysis on the excitation wavelength dependence presented at the ensemble level in **Fig. 4**.

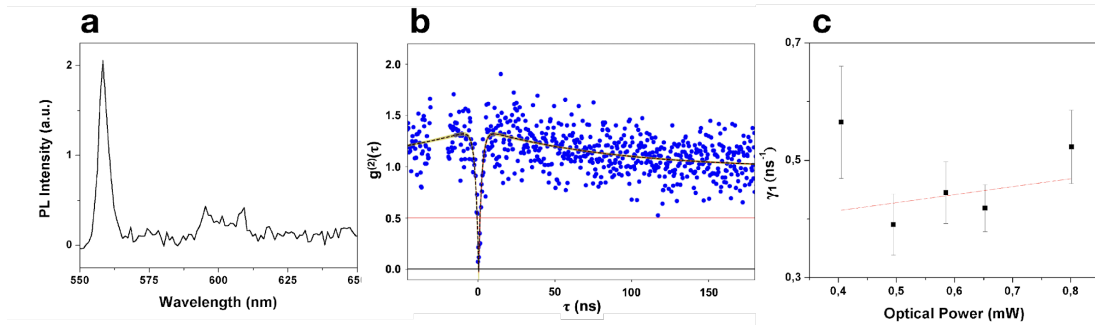


Figure 7: Investigation of single-photon emission from MgV centers at 7 K temperature: **a)** Background-subtracted PL spectrum acquired from an individual emitter under 522 nm optical excitation (4.6 mW); **b)** second-order autocorrelation function acquired from the same emitter under 0.7 mW excitation power; **c)** dependence of the γ_1 emission parameters on the optical excitation power. The excited lifetime for the emitter was estimated as (2.8 ± 1.1) ns according to eq. (1).

Conclusions

This work offers a first systematic experimental analysis of the structural and photo-physical properties of MgV centers fabricated upon ion implantation, following the first report on their optical activity²⁵ and the development of a first theoretical model.²⁶

The emission channeling analysis of ²⁷Mg-implanted diamond revealed a high fraction of Mg (30-42%) in sites that are compatible with the split-vacancy configuration proposed as the structure of the relevant optically-active center. This indicates the very efficient structural formation of MgV, which appears comparable to that of the SnV defect.³¹

The spectral features of MgV centers at both room-temperature and cryogenic temperatures also confirmed the signature of ZPL at 557.6 nm attributed to the ${}^2E_u^{(2)} \rightarrow {}^2E_g$ optical transition. The temperature dependence of this emission line showed a peculiar, counter-intuitive blue-shift, which is unprecedented in the landscape of solid-state quantum emitters. This effect was interpreted in terms of an increased occupation probability of the 4E_u state.

The analysis also showed previously unexplored emission properties, including the occurrence of a previously unreported line at 608.3 nm at cryogenic temperatures, compatible with the ${}^2A_{1u} \rightarrow {}^2E_g$ transition predicted in Ref. 26, and the persistence of the 544 nm emission under all the considered excitation wavelengths in undoped substrates (in disagreement with the results in Ref. 35).

Finally, the single-photon emitter analysis of MgV centers suggests an appealing excited state radiative lifetime (2.7 ± 0.3) ns, paired with a bright emission rate in reaching, in the saturation regime, up to (1.46 ± 0.17) Mcps under (2.7 ± 0.4) mW Raman-resonant excitation power, despite a large variability in the data distribution. The highest measured emission intensity at saturation is larger than that of the most intense group-IV impurity related defects (SnV, PbV)^{15,17}, at > 1 Mcps rates, and tops them by a factor of two under resonant excitation if the specific spectral transmittance of the experiment is taken into account. The results presented here on the intense emission, the efficient structural formation of the defect exploiting ion implantation and the high Debye-Waller factor, combined with the enticing spin-dependent properties for the center’s ground state²⁶, offer an enticing perspective of practical applications of the MgV center in quantum technologies as a bright qubit for quantum sensing and quantum information processing.

Acknowledgements

This work was supported by the following projects: ‘Intelligent fabrication of QUANTum devices in DIAMOND by Laser and Ion Irradiation’ (QuantDia) project funded by the Italian Ministry for Instruction, University and Research within the ‘FISR 2019’ program; ‘Training on LASer fabrication and ION implantation of DEFects as quantum emitters’ (LasIonDef) project funded by the European Research Council under the ‘Marie Skłodowska-Curie Innovative Training Networks’ program; experiments ROUGE and QUANTEP, funded by the 5th National Commission of the Italian National Institute for Nuclear Physics (INFN); Project “Piemonte Quantum Enabling Technologies” (PiQuET), funded by the Piemonte Region within the “Infra-P” scheme (POR-FESR 2014-2020 program of the European Union); “Departments of Excellence” (L. 232/2016), funded by the Italian Ministry of Education, University and Research (MIUR); “Ex post funding of research - 2021” of the University of Torino funded by the “Compagnia di San Paolo”; The projects 20IND05 (QADeT) and 20FUN05 (SEQUME) leading to this publication have received funding from the EMPIR programme co-financed by the Participating States and from the European Union’s Horizon 2020 research and innovation programme. J.F. gratefully acknowledge the EU RADIATE Project (grant ID 824096; proposal 20002351-ST) for granting transnational access to the IMBL laboratory at KU Leuven.

A.C., G.M., J.M., S.M.T., R.V., A.V., L.M.C.P. acknowledge support from the KU Leuven and the Research Foundation – Flanders (FWO, Belgium).

We appreciate the support of the ISOLDE Collaboration and technical teams. This work was funded by the Portuguese Foundation for Science and Technology (Fundação para a Ciência e a Tecnologia FCT, CERN/FIS-TEC/0003/2019). The EU Horizon 2020 Framework supported ISOLDE beam times through Grant Agreement No. 654002 (ENSAR2).

The authors would like to express their gratitude to Optoprim Srl and nLight for their collaboration and technical support.

References

1. T. Schröder, S.L. Mouradian, J. Zheng, M.E. Trusheim, M. Walsh, E.H. Chen, L. Li, I. Bayn, D. Englund, Quantum nanophotonics in diamond, *Journal of the Optical Society of America B* **33** (4), B65 (2016).
2. I. Aharonovic, D. Englund, M. Toth, Solid-state single-photon emitters, *Nat. Photonics* **10**, 631 (2016).
3. D. Chen, N. Zheludev, W. Gao, Building Blocks for Quantum Network Based on Group-IV Split-Vacancy Centers in Diamond, *Adv. Quantum Techn.* **3**, 1900069 (2020).
4. M.W. Doherty, N.B. Manson, P. Delaney, F. Jelezko, J. Wrachtrup, L.C.L. Hollenberg, The nitrogen-vacancy colour centre in diamond, *Phys. Rep.* **528**, 1 (2013).
5. K. Tsurumoto, R. Kuroiwa, H. Kano, Y. Sekiguchi, H. Kosaka, Quantum teleportation-based state transfer of photon polarization into a carbon spin in diamond, *npj Commun. Phys.* **2**, 74 (2019)
6. F. Dolde, M.W. Doherty, J. Michl, I. Jakobi, B. Naydenov, S. Pezzagna, J. Meijer, P. Neumann, F. Jelezko, N.B. Manson, J. Wrachtrup, Nanoscale detection of a single fundamental charge in ambient conditions using the NV⁻ center in diamond, *Phys. Rev. Lett.* **112**, 097603 (2014).
7. A. Sipahigil, M.L. Goldman, E. Togan, Y. Chu, M. Markham, D.J. Twitchen, A.S. Zibrov, A. Kubanek, M.D. Lukin, Quantum interference of single photons from remote nitrogen-vacancy centers in diamond, *Phys. Rev. Lett.* **108**, 143601 (2012).
8. S. Pezzagna, J. Meijer, Quantum computer based on color centers in diamond, *Appl. Phys. Rev.* **8**, 011308 (2021).
9. G. Petrini, G. Tomagra, E. Bernardi, E. Moreva, P. Traina, A. Marcantoni, F. Picollo, K. Kvakova, P. Cigler, I.P. Degiovanni, V. Carabelli, M. Genovese, Nanodiamond quantum sensors reveal temperature variation associated to hippocampal neurons firing, *Adv. Science* **9**, 2202014 (2022).
10. C. Bradac, W. Gao, J. Forneris, M.E. Trusheim, I. Aharonovich, Quantum nanophotonics with group IV defects in diamond, *Nat. Comm.* **10**, 5625 (2019).
11. C. Wang, C. Kurtsiefer, H. Weinfurter, B. Burchard, Single photon emission from SiV centres in diamond produced by ion implantation, *J. Phys. B* **39**, 37 (2006).
12. T. Müller, C. Hepp, B. Pingault, E. Neu, S. Gsell, M. Schreck, H. Sternschulte, D. Steinmüller-Nethl, C. Becher, M., Atatüre, Optical signatures of silicon-vacancy spins in diamond, *Nat. Commun.* **5**, 3328 (2014).

13. Y.N. Palyanov, I.N. Kupriyanov, Y.M., Borzdov, N. V. Surovtsev, Germanium: a new catalyst for diamond synthesis and a new optically active impurity in diamond, *Sci. Reports* **5**, 14789 (2015).
14. T. Iwasaki, F. Ishibashi, Y. Miyamoto, Y. Doi, S. Kobayashi, T. Miyazaki, K. Tahara, K.D. Jahnke, L.J. Rogers, B. Naydenov, F. Jelezko, S. Yamasaki, S. Nagamachi, T. Inubushi, N. Mizuochi, M. Hatano, Germanium-Vacancy Single Color Centers in Diamond, *Sci. Reports* **5**, 12882 (2015).
15. S. Ditalia Tchernij, T. Herzig, J. Forneris, J. Küpper, S. Pezzagna, P. Traina, E. Moreva, I.P. Degiovanni, G. Brida, N. Skukan, M. Genovese, M. Jaksic, J. Meijer, P. Olivero, Single-Photon-Emitting Optical Centers in Diamond Fabricated upon Sn Implantation, *ACS Photonics* **4**, 2580 (2017).
16. T. Iwasaki, Y. Miyamoto, T. Taniguchi, P. Siyushev, M.H. Metsch, F. Jelezko, M. Hatano, M., Tin-Vacancy Quantum Emitters in Diamond, *Phys. Rev. Lett.* **119**, 253601 (2017).
17. S. Ditalia Tchernij, T. Lühmann, T., Herzig, J. Küpper, A. Damin, S. Santonocito, M. Signorile, P. Traina, E. Moreva, F. Celegato, S. Pezzagna, I.P. Degiovanni, P. Olivero, M. Jaksic, J. Meijer, M. Genovese, J. Forneris, Single-Photon Emitters in Lead-Implanted Single-Crystal Diamond, *ACS Photonics* **5**, 4864 (2018).
18. M.E. Trusheim, H.N. Wan, K.C. Chen, C.J. Ciccarino, J. Flick, R. Sundararaman, G. Malladi, E. Bersin, M. Walsh, B. Lienhard, H. Bakhru, P. Narang, D. Englund, Lead-related quantum emitters in diamond, *Phys. Rev. B* **99**, 075430 (2019).
19. A.M. Zaitsev, *Optical Properties of Diamond – Data Handbook*, Springer, Berlin, Heidelberg (2001).
20. G. Prestopino, M. Marinelli, E. Milani, C. Verona, G. Verona-Rinati, P. Traina, E. Moreva, I. P. Degiovanni, M. Genovese, S. Ditalia Tchernij, F. Picollo, P. Olivero, J. Forneris, Photo-physical properties of He-related color centers in diamond, *Appl. Phys. Lett.* **111**, 111105 (2017).
21. R. Sandstrom, L. Ke, A. Martin, Z. Wang, M. Kianinia, B. Green, W. Gao, I. Aharonovich, Optical properties of implanted Xe color centers in diamond, *Optics Commun.* **411**, 182-186 (2018).
22. I. Aharonovich, S. Castelletto, B. C. Johnson, J. C. McCallum, D. A. Simpson, A. D. Greentree, and S. Praver, Chromium single-photon emitters in diamond fabricated by ion implantation, *Phys. Rev. B* **81**, 121201 (2010).
23. T. T. Gaebel, I. Popa, A. Gruber, M. Domhan, F. Jelezko, and J. Wrachtrup, Stable single-photon source in the near infrared, *New J. Phys.* **6**, 98 (2004).
24. S. Ditalia Tchernij, T. Lühmann, E. Corte, , F. Sardi, F. Picollo, P. Traina, M. Brajković, A. Crnjac, S. Pezzagna, Ž. Pastuović, I. P. Degiovanni, E. Moreva, P. Aprà, P. Olivero, Z. Siketić, J. Meijer, M. Genovese, J. Forneris, Fluorine-based color centers in diamond. *Sci. Rep.* **10**, 21537 (2020).
25. T. Lühmann, N. Raatz, R. John, M. Lesik, J. Rödiger, M. Portail, D. Wildanger, F. Kleiβler, K. Nordlund, A. Zaitsev, J.-F. Roch, A. Tallaire, J. Meijer, S. Pezzagna, Screening and engineering of colour centres in diamond., *J. Phys. D: Appl. Phys.* **51**, 483002 (2018).
26. A. Pershin, G. Barcza, Ö. Legeza, A. Gali, Highly tunable magneto-optical response from magnesium-vacancy color centers in diamond. *npj Quantum Inf.* **7**, 99 (2021).

27. H. Hofsäss, G. Lindner, Emission channeling and blocking, *Phys. Rep.* **201**, 121 (1991).
28. U. Wahl, Advances in electron emission channeling measurements in semiconductors, *Hyperfine Interact.* **129**, 349 (2000).
29. U. Wahl, J. G. Correia, A. Czermak, S. Jahn, P. Jalocha, J. Marques, A. Rudge, F. Schopper, J. C. Soares, A. Vantomme, Position-sensitive Si pad detectors for electron emission channeling experiments, *Nucl. Instrum. Methods Phys. Res., Sect. A* **524**, 245 (2004).
30. L. M. C. Pereira, A. Vantomme, U. Wahl, Characterizing defects with ion beam analysis and channeling techniques, in *Characterisation and Control of Defects in Semiconductors*, edited by F. Tuomisto (Institution of Engineering and Technology, Stevenage, UK, 2019), Chap.11, pp. 501–563.
31. U. Wahl, J. G. Correia, R. Villarreal, E. Bourgeois, M. Gulka, M. Nesládek, A. Vantomme, and L. M. C. Pereira, Direct structural identification and quantification of the split-vacancy configuration for implanted Sn in diamond, *Phys. Rev. Lett* **125** (2020) 045301.
32. U. Wahl, L. M. Amorim, V. Augustyns, A. Costa, E. David-Bosne, T. A. L. Lima, G. Lippertz, J. G. Correia, M. R. da Silva, M. J. Kappers, K. Temst, A. Vantomme, and L. M. C. Pereira, Lattice Location of Mg in GaN: A Fresh Look at Doping Limitations, *Phys. Rev. Lett.* **118**, 095501 (2017).
33. U. Wahl, J.G. Correia, A.R.G. Costa, E. David-Bosne, T.A.L. Lima, G. Lippertz, A. Vantomme, M.R. da Silva, M.J. Kappers, and L.M.C. Pereira, Lattice location studies of the amphoteric nature of implanted Mg in GaN, *Adv. Electron. Mater.* **7**, 2100345 (2021).
34. E. David-Bosne, U. Wahl, J. G. Correia, T. A. L. Lima, A. Vantomme, and L. M. C. Pereira, A generalized fitting tool for analysis of two-dimensional channeling patterns, *Nucl. Instrum. Methods Phys. Res., Sect. B* **462**, 102 (2020)
35. T. Lüthmann, R. John, R. Wunderlich, J. Meijer, S. Pezzagna, Coulomb-driven single defect engineering for scalable qubits and spin sensors in diamond, *Nat. Commun.* **10**, 4956 (2019).
36. A.A. Razgulov, S. G. Lyapin, A.P. Novikov, E.A. Ekimov, Low-temperature photoluminescence study of SnV centers in HPHT diamond, *Diam. Relat. Mater.* **116**, 108379 (2021).
37. M.W. Doherty, V.M. Acosta, A. Jarmola, M.S.J. Barson, N.B. Manson, D. Budker, L.C.L. Hollenberg, Temperature shifts of the resonances of the NV⁻ center in diamond, *Phys. Rev. B.* **90**, 041201 (2014).
38. B. Dong, C. Shi, Z. Xu, K. Wang, H. Luo, F. Sun, P. Wang, E. Wu, K. Zhang, J. Liu, Y. Song, Y. Fan, Temperature dependence of optical centers in Ib diamond characterized by photoluminescence spectra, *Diam. Relat. Mater.* **116**, 108389 (2021).
39. J.-W. Fan, I. Cojocaru, J. Becker, I.V. Fedotov, M. Hassan, A. Alkahtani, A. Alajlan, S. Blakley, M. Rezaee, A. Lyamkina, Y.N. Palyanov, Y.M. Borzdov, Y.-P. Yang, A. Zheltikov, P. Hemmer, A.V. Akimov, Germanium-Vacancy Color Center in Diamond as a Temperature Sensor, *ACS Photonics* **5**, 765 (2018).

40. Thorlabs Longpass Dichroic Mirrors/Beamsplitters website. Long-pass dichroic mirror, model DMLP567. https://www.thorlabs.com/newgrouppage9.cfm?objectgroup_id=3313. (accessed 2022-10-25).
41. J.N. Becker, J. Görlitz, C. Arend, M. Markham, C. Becher, Ultrafast all-optical coherent control of single silicon vacancy colour centres in diamond, *Nat. Commun.* **7**, 13512 (2016)
42. S. C. Kitson, P. Jonsson, J. G. Rarity, P. R. Tapster, Intensity fluctuation spectroscopy of small numbers of dye molecules in a microcavity *Phys. Rev. A* **58**, 620 (1998).
43. E. Corte, S. Sachero, S. Ditalia Tchernij, T. Lühmann, S. Pezzagna, P. Traina, I.P. Degiovanni, E. Moreva, P. Olivero, J. Meijer, M. Genovese, J. Forneris, Spectral Emission Dependence of Tin-Vacancy Centers in Diamond from Thermal Processing and Chemical Functionalization, *Adv. Photonics Res.* **2021**, 2100148 (2021).
44. C. Kurtsiefer, S. Mayer, P. Zarda, H. Weinfurter, Stable Solid-State Source of Single Photons, *Phys. Rev. Lett.* **85**, 290 (2000).
45. I. Aharonovich, S. Castelletto, D.A. Simpson, A. Stacey, J. McCallum, A.D. Greentree, S. Praver, Two-Level Ultrabright Single Photon Emission from Diamond Nanocrystals. *Nano Lett.* **9**, 3191 (2009).
46. E. Neu, D. Steinmetz, J. Riedrich-Möller, S. Gsell, M. Fischer, M. Schreck, C. Becher, Single photon emission from silicon- vacancy colour centres in chemical vapour deposition nano-diamonds on iridium. *New J. Phys.* **13**, 025012 (2011).